ADVANCED FUNCTIONAL MATERIALS
www.afm-journal.de

Chiral Mechanical Metamaterials for Tunable Optical Transmittance

Antonio Elia Forte, David Melancon, Mohamed Zanati, Marta De Giorgi, and Katia Bertoldi**

Flexible metamaterials have been increasingly harnessed to create functionality through their tunable and unconventional response. Herein, chiral unit cells based on Archimedean spirals are employed to transform a linear displacement into twisting. First, the effect of geometry on such extension-twisting coupling is investigated. This unravels a wide range of highly nonlinear behaviors that can be programmed. Additionally, it is demonstrated that by combining the spirals with polarizing films one can create mechanical pixels capable of modulating the transmission of light through deformation. Guided by experiments and numerical analyses, pixels are arranged in 2D arrays to realize black and white and color displays, which reveal distinct images at different states of deformation. As such, the study puts forward a methodology for the design of an emerging class of flexible devices that can convert nonlinear elastic deformation to tunable optical transmittance.

1. Introduction

The ability to tune the optical transmittance of materials and structures opens new paths to a range of innovative applications, including flexible strain sensors,[1] skins for camouflage[2] and displays.[3] To achieve such an optical response, a number of artificial compounds have been synthesized. In these 'chromogenic' materials changes in the environmental conditions (such as temperature, light, stress, pH) alter the equilibrium of electrons and, consequently, lead to a change in color.[4] Optical properties can also be tuned by embedding a variety of microscale features like pillars,[5] opaque platelets,[6] holes,[7] and particles[8–10] into clear elastomers (e.g., polydimethylsiloxane - PDMS). However, fabrication of microscale structures is challenging and the inclusion of stiffer elements reduces devices' life, as these can tear the elastomeric medium.

Mechanical metamaterials with carefully designed architectures offer avenues to achieve deformation modes that are inaccessible with ordinary materials.[11–14] For example, metamaterials based on a 3D chiral unit cells can twist in response to an applied uniaxial load, which never happens in ordinary continuum materials.[15] These unusual deformation modes can be exploited for space satellites and telescopes actuation,[16] sound absorption,[17] and vibration attenuation.[18]

Taking inspiration from this, here we focus on an initially flat elastic spiral that twists when pulled out-of-plane (see **Figure 1**a). We first show that this extension-twisting coupling can be largely tuned by varying the geometry of the spiral. Then, we exploit this coupling to realize a mechanical pixel capable of modulating light through elastic deformation. To this end, we employ polarized films and combine them with the spirals in order to control their rotation, as the amount of light that passes through these films depends on how they are rotated in relation to one another (see Figure 1b). As we apply the out-of-plane displacement, the unit cell twists and drives one of the polarizer, decreasing the amount of light transmitted (see Figure 1c). Finally, we rationally combine these pixels to realize a mechanical black and white display capable of rendering distinct images at different deformation states. As such, our study introduces a simple strategy to tune optical transmittance by exploiting the complex 3D elastic deformation of structures. Although there are inexpensive and well established approaches to manufacture displays (e.g., liquid-crystal displays), the devices we hereby propose are expected to be suited for applications at low temperatures and/or electronic-free conditions, as their deployment is driven by geometry and could be triggered by various types of actuation (e.g., motor-drive, pneumatic, shape-memory alloys, magnetic field).

A. E. Forte, D. Melancon, M. Zanati, K. Bertoldi
J.A. Paulson School of Engineering and Applied Sciences
Harvard University
Cambridge, MA 02138, USA
E-mail: antonio.forte@kcl.ac.uk; bertoldi@seas.harvard.edu

A. E. Forte
Department of Engineering
King's College London
London WC2R 2LS, UK

D. Melancon
Department of Mechanical Engineering
Polytechnique Montreal
Quebec H3T 1J4, Canada

M. De Giorgi
Department of Engineering for Innovation
University of Salento
Lecce 73100, Italy

The ORCID identification number(s) for the author(s) of this article can be found under https://doi.org/10.1002/adfm.202214897.

DOI: 10.1002/adfm.202214897

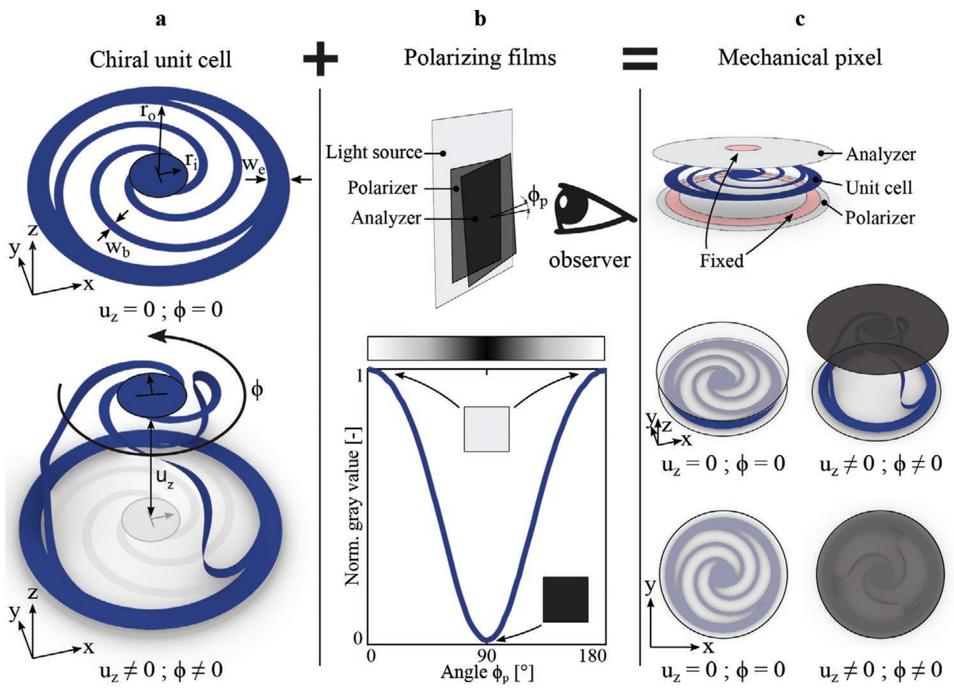

Figure 1. Chiral mechanical metamaterials for tunable optical transmittance. a) The chiral unit cell: a spiral that twists when pulled out-of-plane. b) Polarizing films filter the amount of light transmitted from the source to the observer depending on their mutual rotation. c) A mechanical pixel is realized by combining the spirals with polarizing films. When an out-of-plane displacement is applied to the mechanical pixel, it twists and modulates the transmission of light.

2. Results

2.1. Our Chiral Unit Cell

Our building block is an Archimedean spiral, laser-cut from a flat 2D sheet and connected on each side to polarizing films. This chiral unit cell comprises three beams with rectangular cross section $w_b \times h$ and centerline r that follows the equation

$$r(\theta)=\frac{r_o \cdot \theta}{\Theta}, \quad \text{with } \theta \in [0,\Theta] \tag{1}$$

where r_o is the outer radius and Θ the angle spanned by the spiral (see Figure 1a). To allow for clamping and loading, we add a circular ring of width w_e along the outer edge of the spiral and an inner circle of radius r_i to its center. Note that the latter modification effectively reduces the length of the beams and affects their deployment.

To investigate the mechanical response of the spirals, we conduct finite element (FE) analyses with the commercial package ABAQUS 2019/Standard. In our simulations, we discretize the spiral with four-node linear shell elements with reduced integration (Abaqus element type S4R), assume an out-of-plane thickness of $t = 0.3$ mm and use a linear elastic material model with Young's modulus $E = 4.23$ GPa and Poisson's ratio, $\nu = 0.4$. We load the spirals by applying an out-of-plane displacement $u_z = 30$ mm to their inner circle, while constraining all degrees of freedom on their outer ring. In Figure 1a, we consider a spiral with $r_i = 5.5$ mm, $w_b = 1.7$ mm, $w_e = 4$ mm, $r_o = 20$ mm, and $\Theta = 360°$ and show the numerically predicted configuration upon application of the out-of-plane displacement. As recently reported for chiral metamaterials,[15] we find that our unit cell twists as it is pulled out-of-plane—therefore exhibiting extension-twisting coupling. To better understand this behavior, in **Figure 2**, we report the evolution of the twisting angle, ϕ, as a function of u_z (see black dashed line) and find a highly nonlinear response. The rotation ϕ remains close to zero up to $u_z = 25$ mm and then suddenly increases to $\phi = 100°$.

To unravel the rich behaviour of the system, we explore the design space and investigate the effect of geometry on ϕ. We start by simulating 117 spirals with $\Theta = 360°$, $r_o = 20$ mm, $t = 0.3$ mm and varying inner circle radius and cross sectional width ($r_i \in [5.5, 13.5]$ mm and $w_b \in [1.5, 4]$ mm). For these spirals we find that three distinct behaviors emerge depending primarily on the value of r_i, since the inner radius effectively dictates the length of the curved beams forming our unit cells (see Figures S5–S7, Supporting Information, for the effect of w_b and additional contour plots): (*i*) for $5.5 \leq r_i < 7$ mm, a nonlinear response similar to that reported for the spiral considered in Figure 1a emerges (see red curves in Figure 2a –this is because such small values of r_i result in slender curved beams which are prone to buckling under compression when the inner circle twists in the counter-clockwise direction, leading to a sudden increase of ϕ upon loading); (*ii*) for $7 \leq r_i < 10$ mm, the ϕ-u_z curves are smoother and "J-shaped" (see blue curves in Figure 2a) as previously described in the literature for chiral metamaterials;[15] (*iii*) for $10 \leq r_i \leq 13.5$ mm, the ϕ-u_z curves are still "J-shaped", but with ϕ initially increasing at a faster rate and then eventually plateauing (see green curves in Figure 2a).

We next increase the length of the beams by setting $\Theta = 720°$ and simulate 81 additional spirals (note the smaller number of spiral designs since some geometries degenerate into a solid disk with $\Theta = 720°$) with $r_o = 20$ mm, $t = 0.3$ mm, and

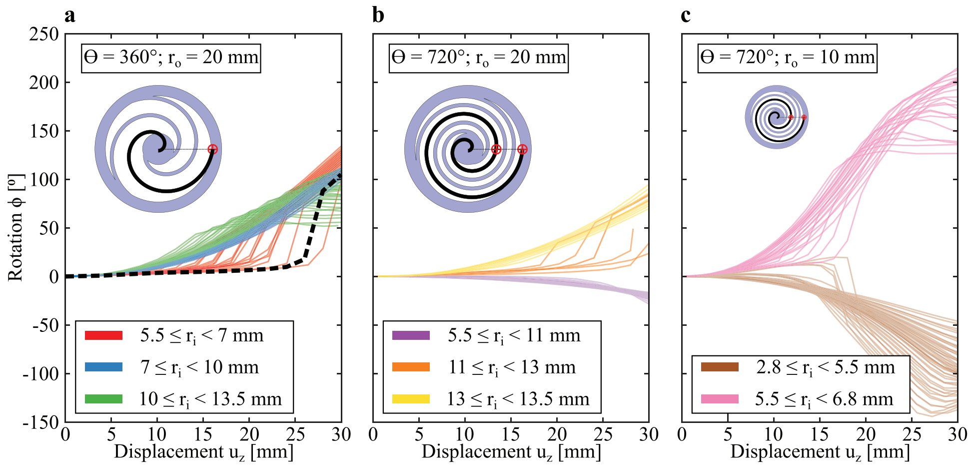

Figure 2. Deformation of the spirals upon loading. Evolution of the twisting angle ϕ as a function of the applied displacement u_z for spirals $t = 0.3$ mm, $r_i \in [2.8, 13.5]$ mm, $w_b \in [0.8, 4]$ mm and $(\Theta, r_o) = (360°, 20\text{mm})$ a), $(720°, 20\text{mm})$ b) , and $(720°, 10\text{mm})$ c).

varying inner circle radius and cross sectional width ($r_i \in [5.5, 13.5]$ mm and $w_b \in [1.5, 3]$ mm). For these spirals, we still find ϕ-u_z curves of type (*i*) and (*ii*) for $11 \le r_i < 13$ mm (see orange curves in Figure 2b) and $13 \le r_i < 13.5$ mm (see yellows curves in Figure 2b), respectively. However, for $5.5 \le r_i < 11$ mm (i.e., extremely slender beams) small rotations in the opposite direction are found since a soft mode of deformation emerges (see purple curves in Figure 2b and Section S4, Supporting Information, for details).

Finally, our simulations indicate that the rotation of the inner circle upon application of $u_z = 30$ mm can be amplified by reducing the outer radius to $r_o = 10$ mm and considering $w_b \in [0.8, 2.0]$ mm, while keeping $\Theta = 720°$ and $t = 0.3$ mm. Also for this case, we simulate 81 spirals and find that rotation angles above 180° can be achieved for $5.5 \le r_i < 6.8$ mm (see pink curves in Figure 2c). Differently, for $2.8 \le r_i < 5.5$ mm, the inner circles rotate in the opposite direction by about ≈100° upon loading.

To experimentally validate our analyses, we fabricate eight different spiral geometries (see **Figure 3**a for their geometric parameters) by laser cutting the 2D pattern out of 0.3 mm-thick Mylar sheets. In all our experiments, we attach the outer ring

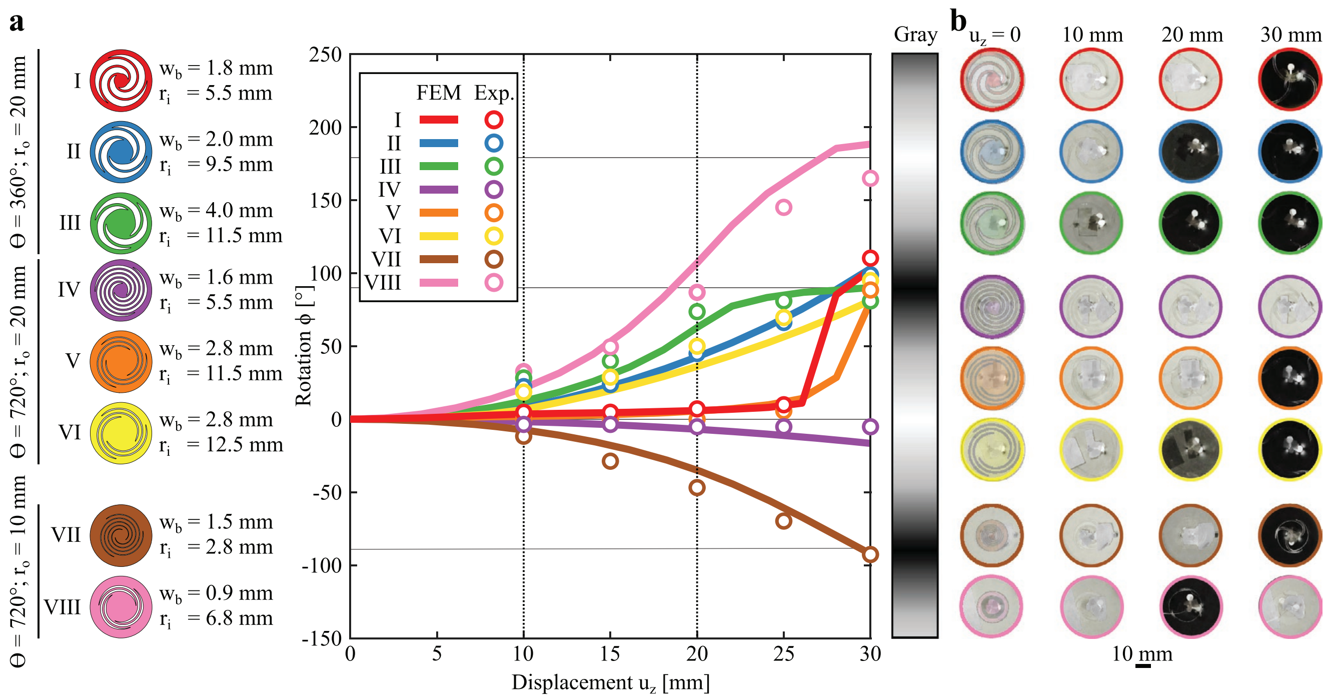

Figure 3. Mechanical pixel. a) ϕ-u_z curves as predicted by FE analyses (continuous lines) and measured in experiments (markers) for eight spirals with $t = 0.3$ mm and (Θ, r_o, r_i, w_b)= (*I*) (360°, 20 mm, 5.5 mm,1.8 mm), (*II*) (360°, 20 mm, 9.5 mm, 2.0 mm), (*III*) (360°, 20 mm, 11.5 mm, 4.0 mm), (*IV*) (720°, 20 mm, 5.5 mm,1.6 mm), (*V*) (720°, 20 mm, 11.5 mm, 2.8 mm), (*VI*) (720°, 20 mm, 12.5 mm, 2.8 mm), (*VII*) (720°, 10 mm, 2.8 mm,1.5 mm), and (*VIII*) (720°, 10 mm, 6.8 mm, 0.9 mm). b) Top view pictures of the mechanical pixels realized by connecting the eight spirals to two polarizing films at $u_z = 0$, 10, 20 and 30 mm.

of the spirals to an acrylic plate via bolts and connect the center of their inner circle to a thread. We then fix the acrylic plate in space and pull on the thread to apply the displacement u_z while leaving the spirals free to rotate (see, Sections S1 and S2, Supporting Information, for details). To track the rotation, ϕ, we cut a reference line on the inner circle of each spiral and monitor its position during the tests using a digital camera (SONY RX100 V) placed above the sample. The camera was manually set at a F11 aperture, 1/100 s shutter speed and ISO on AUTO. All the data were collected at night, in a dark room with no environmental lighting. The camera was placed on a tripod at a distance of 50 cm from the sample. The sample was placed on 60×60 cm back-lit LED panel with a white temperature of 5500 K, power of 40 W and an luminous flux of 4000 lm (LIFUD UGR19). As shown in Figure 3b, we find good agreement between simulations and experiments, with measured twisting angles ϕ that closely follow the numerically predicted ones.

2.2. From Chiral Unit Cells to Mechanical Pixels

Thus far, we have shown that the geometry of the spirals strongly affect their coupled extension-twisting behavior. We now show how to harness such behavior to create a device that can modulate light. To this end, we bond (using cyanoacrilate) two circular polarizing films (Izgut High Contrast Linear Polarizing Film) with radius r_o to the spirals: one to the outer ring and one to the inner circle on the opposite face. When these films are irradiated with a light source, the amount of light that goes through them and reaches an observer, positioned opposite to it, depends on their mutual rotation. In particular, the intensity of the light transmitted, I_t, is given by Malus's law:[19]

$$I_t = I_0 \cos^2(\phi_p) \tag{2}$$

where I_0 is the intensity of the light emitted from the source and ϕ_p denotes the angle between the transmission axes of the two films. In all our sample we orient the polarizing films so that in the flat configurations (i.e., for $u_z = 0$) they are perfectly aligned (i.e., $\phi_p = 0$) and let through the maximum light intensity (i.e., $I_t = I_0$). However, the inner circle rotates as we apply the out-of-plane displacement u_z and makes the film connected to it rotate by the same amount (i.e., $\phi_p = \phi$), reducing the light transmitted. In Figure 3b, we show top view pictures of the eight considered mechanical pixels (i.e., the spirals coupled with the polarizing films) at $u_z = 0$, 10, 20, and 30 mm. As expected, all of the mechanical pixels are white in the flat configuration, since $\phi = 0$ and the intensity of the transmitted light is maximized. However, due to the extension-twisting coupling of the spirals, all pixels become darker as the displacement u_z is applied with the exception of the spiral characterized by $\Theta = 720°$, $r_o = 20$ mm, $w_b = 1.6$ mm, and $r_i = 5.5$ mm, for which $|\phi| < 10°$ for the considered range of applied displacement. It is important to point out that the relation between the twist angle ϕ and the applied displacement u_z for the spirals completely dictates the optical behavior of our pixels. Spirals that display a sudden increase in ϕ result in pixels displaying a sudden transition from white to black, whereas spirals that exhibit smooth increase of ϕ lead to pixels that display a smooth transition from white to black. Further, spirals that rotate more than 180° (see spiral with $\Theta = 720°$, $r_o = 10$ mm, $w_b = 0.9$ mm, and $r_i = 6.8$ mm in Figure 3) enable realization of pixels that first transition from white to black and then eventually go back to white (when ϕ reaches 180°).

2.3. Black and White Mechanical Displays

The results of Figure 3 indicate that our design space allows us to build chiral mechanical pixels that can transition from white to black, or from white to black and back to white, or stay white. Here, we show how to combine such pixels to create a mechanical black and white display. To demonstrate the concept, we focus on a 5×5 array of pixels and assume that all 25 spirals are subjected to the same displacement u_z. Note that thanks to the rich non-linear behavior of the spirals, even under this homogeneous loading condition multiple images can be encoded into the display and be revealed at different levels of applied displacement. As an example, here we look for an arrangement of pixels that displays (see **Figure 4**a): (1) a white square in the undeformed configuration (i.e., for $u_z = 0$); (2) a black letter "L" on a white background for $u_z = u_1$; (3) a black letter "S" on a white background $u_z = u_2$ with $u_2 > u_1$. Such mechanical display requires four different types of pixels: (Pixel I) that remains white up to $u_z = u_2$ (see pixels highlighted in gray in Figure 4a); (Pixel II) that becomes black at $u_z = u_1$ and remain black up to $u_z = u_2$ (see pixels highlighted in red in Figure 4a) (Pixel III) that is black at $u_z = u_1$ and returns white for $u_z = u_2$; (see pixels highlighted in green in Figure 4a); and (Pixel IV) that is white at $u_z = u_1$ and becomes black at $u_z = u_2$ (see pixels highlighted in blue in Figure 4a). As the polarized sheets become the darkest when rotated of 90° in respect to each other, and the lightest when rotated of 180°, these four distinct optical behaviors can be achieved using spirals for which

$$\text{Pixel } \alpha: \left|\phi\left(u_z = u_i\right)\right| = \phi^{\alpha}_{u_i}, \quad i = 1, 2 \tag{3}$$

where $\alpha = I$, II, III and IV and

$$\begin{array}{llll} \text{Pixel I}: & \phi^{I}_{u_1} = 0° & \text{and} & \phi^{I}_{u_2} = 0°; \\ \text{Pixel II}: & \phi^{II}_{u_1} = 90° & \text{and} & \phi^{II}_{u_2} = 90°; \\ \text{Pixel III}: & \phi^{III}_{u_1} = 90° & \text{and} & \phi^{III}_{u_2} = 180°; \\ \text{Pixel IV}: & \phi^{IV}_{u_1} = 0° & \text{and} & \phi^{IV}_{u_2} = 90° \end{array} \tag{4}$$

To identify such spirals, we inspect our database comprised of 279 different design geometries. More specifically, we consider 200 equally spaced displacements $u_z \in [0, 30]$ mm and then for each pair (u_1, u_2) (with $0 < u_1 < u_2 < 30$ mm) we identify four spirals that minimize:

$$\Psi(u_1, u_2) = \sum_{\alpha=I}^{IV} \left(\left|\phi(u_1)\right| - \left|\phi^{\alpha}_{u_1}\right|\right)^2 + \left(\left|\phi(u_2)\right| - \left|\phi^{\alpha}_{u_2}\right|\right)^2 \tag{5}$$

We find that Ψ is minimum for $u_1 = 20.8$ mm and $u_2 = 26.4$mm and for spirals with (Θ, r_i, r_o, w_b) = (720°, 11.4mm, 20mm, 2.3mm), (360°, 5.4mm, 20mm, 3.9mm), (720°, 6.2mm, 10mm, 0.7mm), (360°, 5.4mm, 20mm, 2.5mm) for Pixels I, II, III, and IV, respectively. We then fabricate these four spirals. As shown in Figure 4c, we find good agreement between the numerical predictions and the experiments. Finally, we use

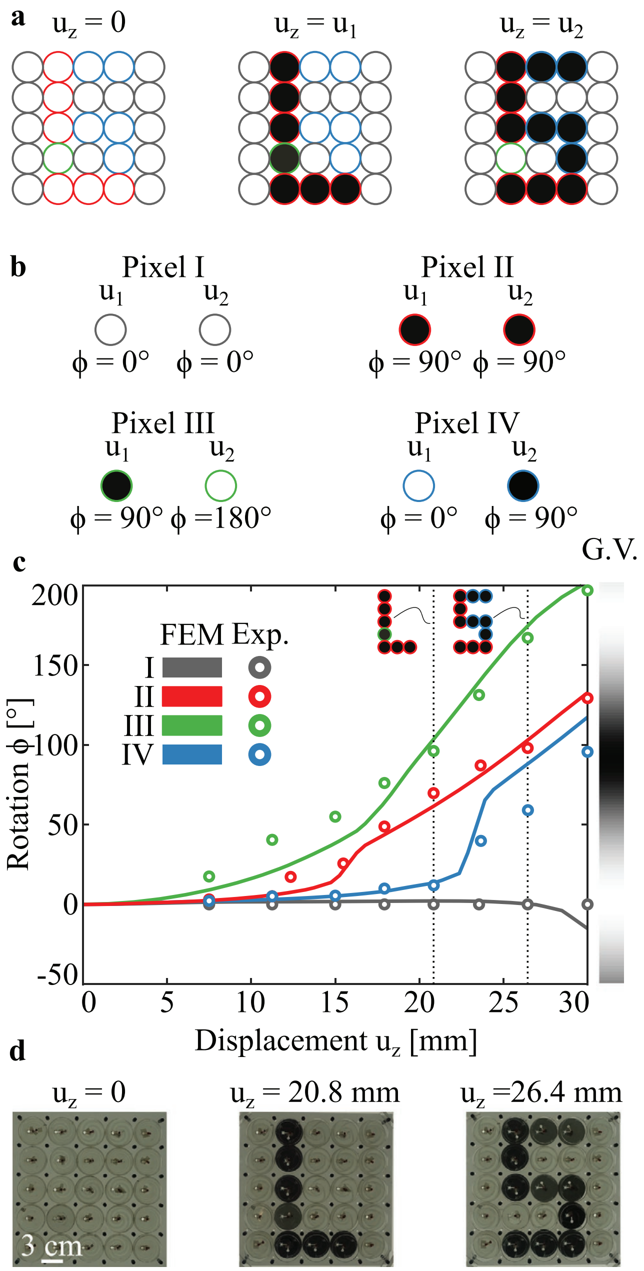

Figure 4. Mechanical display. a) Schematics of a 5 × 5 mechanical display that display (1) a white square for $u_z = 0$, (2) a black letter "L" on a white background for $u_z = u_1$, and (3) a black letter "S" on a white background *for* $u_z = u_2$. b) Four different types of pixel are required to realize such mechanical display. c) FEM-predicted and experimentally measured $\phi - u_z$ curves for the optimal spirals that minimize the error Ψ. d) Top view pictures of the mechancial display showing a transition from white to the letter "L" to the letter "S" as u_z is increased to 20.8 and 26.4 mm.

13, 6, 1, and 5 replicates of Pixel I, II, III, and IV, respectively, to build the 5 × 5 mechanical display of Figure 4a. The display is initially white at $u_z = 0$. As predicted by our numerical model, upon application of an out-of-plane displacement, it then sequentially shows the two programmed images, i.e., the letter "L" at $u_z = 20.8$ mm and the letter "S" at $u_z = 26.4$ mm (see Figure 4d).

2.4. Color Mechanical Displays

While in Figure 4, we have demonstrated our approach on a display comprising 25 black and white pixels, color displays can aso be realized by inserting a retarder (e.g., birefringent tape) between the two polarizing films to induce a double refraction from the incident light passing through the system[20] (see, Section S3, Supporting Information, for details about the methodology). To demonstrate the concept, here we focus on a 5 × 5 array of pixels, all subjected to the same displacement u_z, and look for an arrangement of pixels and birefringent tape layouts that displays (see **Figure 5**a): (1) a red heart on a yellow background for $u_z = u_1$ and (2) a red letter "H" on a blue background for $u_z = u_2$. For this example, the mechanical display require three types of pixels (see Figure 5b): (Pixel Ic) that transitions from the color yellow at $u_z = u_1$ to the color blue at $u_z = u_2$ (see pixels highlighted with a bold contour in Figure 5a); (Pixel IIc) that transitions from the color red at $u_z = u_1$ to the color blue at $u_z = u_2$ (see pixels highlighted with a fine-dashed line contour in Figure 5a); and (Pixel IIIc) that displays the red color at $u_z = u_1$ and remains red at $u_z = u_2$ (see pixels highlighted with a course-dashed line contour in Figure 5a). These three behaviors can be achieved using spirals for which:

$$\text{Pixel } \xi: \Gamma(u_z = u_i) = \Gamma^{\xi}_{u_i}, \quad i = 1,2 \tag{6}$$

where $\xi = Ic$, IIc, and $IIIc$, Γ is a vector function mapping the displacement of the spirals and their birefringent tape layout to the RGB value of the transmitted color, and

$$\begin{aligned}
&\text{Pixel Ic}: && \Gamma^{Ic}_{u_1} = [0.7, 0.7, 0.3] && \text{and} && \Gamma^{Ic}_{u_2} = [0.5, 0.4, 0.3] \\
&\text{Pixel IIc}: && \Gamma^{IIc}_{u_1} = [0.7, 0.2, 0.2] && \text{and} && \Gamma^{IIc}_{u_2} = [0.5, 0.4, 0.3] \\
&\text{Pixel IIIc}: && \Gamma^{IIIc}_{u_1} = [0.7, 0.2, 0.2] && \text{and} && \Gamma^{IIIc}_{u_2} = [0.2, 0.2, 0.2]
\end{aligned} \tag{7}$$

To identify such spirals, we inspect our database comprised of 279 different design geometries (see Figure S3, Supporting Information). For each spiral design, we now have the freedom to apply 60 different tape layouts as listed in Table S1 (Supporting Information). To reduce this large design space and for simplicity, we set $u_1 = 0$. Then, for each combination of spiral geometry and tape layout, we consider 200 equally spaced displacements $u_z \in [0, 30]$ mm and then (since we set $u_1 = 0$), for each possible displacement $u_2 < 30$ mm, we find the three spirals that minimize:

$$\Psi(u_2) = \sum_{\xi = Ic}^{IIIc} \left(\left\| \Gamma(0) - \Gamma^{\xi}_{u_1} \right\|^2 + \left\| \Gamma(u_2) - \Gamma^{\xi}_{u_2} \right\|^2 \right) \tag{8}$$

We find that Ψ is minimum for $u_2 = 29.4$ mm and for spirals with $(\Theta, r_i, r_o, w_b, \gamma_1, \gamma_2)$ = (360°, 13.5mm, 20.0mm, 2.5mm, 150°, –), (720°, 6.5mm, 20.0mm, 3.2mm, 60°, 15°), and (720°, 12.5mm, 20.0mm, 3.2mm, 60°, 15°) for Pixel Ic, IIc, and IIIc, where γ_i denote the angle between the optical axis of the i-th layer of birefringent tape and the global x-axis of the system (see Figure S3, Supporting Information). We then fabricate these three spirals and add the corresponding layers of birefringent tape on them. As shown in Figure 5c, we find good agreement between the numerical predictions and the experiments. Finally, we use 9, 9, and 7 replicates of Pixel Ic, IIc, and IIIc, respectively, to build the 5 × 5 mechanical display of Figure 5a. The display initially shows a red heart on a yellow

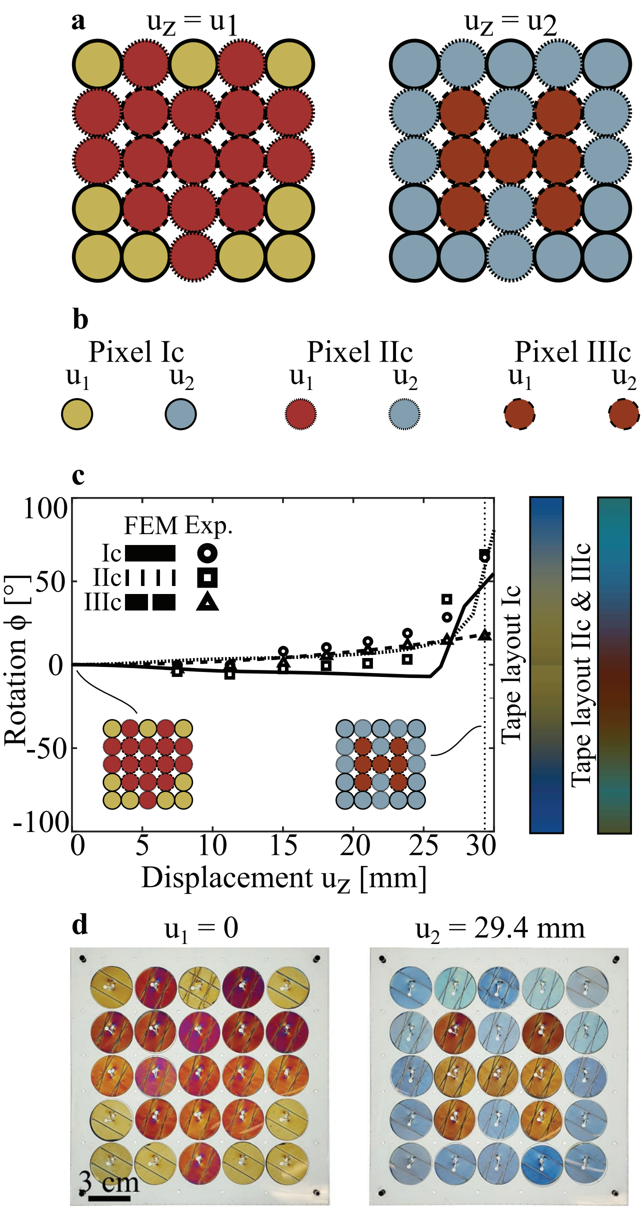

Figure 5. Color display. a) Schematics of a 5 × 5 mechanical display that shows (1) a red heart on a yellow background for $u_z = u_1$, (2) the letter "H" on a blue background for $u_z = u_2$. b) Three different types of pixel are required to realize such color display. c) FEM-predicted and experimentally measured $\phi - u_z$ curves for the optimal spirals and birefringent tape layouts that minimize the error Ψ. d) Top view pictures of the mechanical display showing a transition from the heart to the letter "H" as u_z is increased from 0 to 29.4 mm.

background at $u_z = 0$. As predicted by our numerical model, upon application of an out-of-plane displacement, it then transitions to the second color image, i.e., a red letter "H" on a blue background at $u_z = 29.4$ mm (see Figure 5c). As noticeable from Figure 5c, some variations in the shades of red and blue are present. This are due to the small misalignment that results from manually applying the birefringent tape at a given angle. An automated fabrication procedure would reduce or eliminate such variations.

3. Conclusion

In summary, in this work, we showed that the tension-twisting coupling exhibited by elastic spirals can be exploited to form mechanical pixels that can modulate light intensity through deformation. Afterward, we combined multiple pixels to realize a black and white mechanical display that can be programmed to encode multiple images at specific out-of-plane displacements, globally applied to the display. It is worth noticing that although in this work we highlight the ability of the pixels to reach full opacity/transparency in order to create distinct and recognizable images (i.e., letters "L" and "S" in Figure 4), the pixels do span an entire range of gray values when subjected to an out-of-plane displacement. Hence, applications where intermediate gray scale values are needed are indeed possible, and our system could be programmed to achieve these states. While in this study, we have demonstrated the concept on a display comprising 5 × 5 pixels, the proposed strategy could be readily extended to larger systems to increase the resolution and show more complex images (see Figure S10, Supporting Information). However, this would require advanced fabrication methods to reduce the pixels' size, potentially through advanced additive[21] and laminate[22] manufacturing techniques.

This work opens avenues for easy-to-make and inexpensive mechanical devices whose transmittance properties can be pre-programmed at the unit cell level. As shown, such devices can be used for black/white and colored displays with encoded information, but further applications could include programmable antennas able to create temporary phase gradients at the surface, where the differing phase from each cell interferes constructively/destructively and produces a desired radiation pattern in the far field. Such mechanical displays could meet the requirements for applications at extreme temperatures that are not suitable for electronic components.

4. Experimental Section

Details of the design and fabrication methods were summarized in Section S1 (Supporting Information). The experimental procedure to measure the spirals' rotation, ϕ, as a function of the applied displacement, u_z, was described in Section S2 (Supporting Information). An extension of the methodology to make color displays was presented in Section S3 (Supporting Information). Finally, additional results were provided in Section S4 (Supporting Information).

Supporting Information

Supporting Information is available from the Wiley Online Library or from the author.

Acknowledgements

This work was supported by the National Science Foundation (NSF) through the Designing Materials to Revolutionize and Engineer our Future (DMREF) program under Award No. DMR-1922321 and the Simons Collaboration on Extreme Wave Phenomena Based on Symmetries.

Conflict of Interest

The authors declare no conflict of interest.

Author Contributions

A.E.F. and D.M. contributed equally to this work. A.E.F., D.M., M.Z., and K.B. proposed and developed the research idea. A.E.F. and D.M. designed and fabricated the samples. A.E.F., D.M., and M.D.G. performed the experiments. A.E.F. and D.M. designed the optimization and ran the numerical calculations. A.E.F., D.M., and K.B. wrote the paper. K.B. supervised the research.

Data Availability Statement

The data that support the findings of this study are available in the supplementary material of this article.

Keywords

deployability, mechanical metamaterials, optics

Received: December 21, 2022
Revised: January 30, 2023
Published online:

[1] D. A. Davis, A. Hamilton, J. Yang, L. D. Cremar, D. Van Gough, S. L. Potisek, M. T. Ong, P. V. Braun, T. J. Martínez, S. R. White, J. S. Moore, N. R. Sottos, *Nature* **2009**, *459*, 68.
[2] C. Yu, Y. Li, X. Zhang, X. Huang, V. Malyarchuk, S. Wang, Y. Shi, L. Gao, Y. Su, Y. Zhang, H. Xu, R. T. Hanlon, Y. Huang, J. A. Rogers, *Proc. Natl. Acad. Sci.* **2014**, *111*, 12998.
[3] C. M. Lampert, *Mater. Today* **2004**, *7*, 28.
[4] Q. Guo, X. Zhang, *Composites, Part B* **2021**, *227*, 109434.
[5] S. G. Lee, D. Y. Lee, H. S. Lim, D. H. Lee, S. Lee, K. Cho, *Adv. Mater.* **2010**, *22*, 5013.
[6] F. López Jiménez, P. Upadhyaya, J. Liljenhjerte, P. Reis, S. Kumar, *Extreme Mech. Lett.* **2016**, *9*, 297.
[7] J. Li, J. Shim, J. Deng, J. T. B. Overvelde, X. Zhu, K. Bertoldi, S. Yang, *Soft Matter* **2012**, *8*, 10322.
[8] D. Ge, E. Lee, L. Yang, Y. Cho, M. Li, D. S. Gianola, S. Yang, *Adv. Mater.* **2015**, *27*, 2489.
[9] F. López Jiménez, S. Kumar, P. M. Reis, *Adv. Opt. Mater.* **2016**, *4*, 620.
[10] Y. Zhu, D. S. Antao, R. Xiao, E. N. Wang, *Adv. Mater.* **2014**, *26*, 6442.
[11] K. Bertoldi, V. Vitelli, J. Christensen, M. Van Hecke, *Nat. Rev. Mater.* **2017**, *2*, 1.
[12] A. A. Zadpoor, *Mater. Horiz.* **2016**, *3*, 371.
[13] M. Kadic, G. W. Milton, M. van Hecke, M. Wegener, *Nat. Rev. Phys.* **2019**, *1*, 198.
[14] X. Xia, C. M. Spadaccini, J. R. Greer, *Nat. Rev. Mater.* **2022**, *7*, 683.
[15] T. Frenzel, M. Kadic, M. Wegener, *Science* **2017**, *358*, 1072.
[16] K. Dudek, A. Drzewiński, M. Kadic, *Proc. R. Soc. A* **2021**, *477*, 20200825.
[17] X. An, C. Lai, W. He, H. Fan, *Composites, Part B* **2021**, *224*, 109232.
[18] P. Zhao, K. Zhang, L. Qi, Z. Deng, *Mech. Syst. Signal Process.* **2022**, *180*, 109430.
[19] E. Collett, *Field guide to polarization*, SPIE Press, Bellingham, Wash **2005**.
[20] A. Beléndez, E. Fernández, J. Francés, C. Neipp, *Eur. J. Phys.* **2010**, *31*, 551.
[21] Z. Yan, F. Zhang, F. Liu, M. Han, D. Ou, Y. Liu, Q. Lin, X. Guo, H. Fu, Z. Xie, M. Gao, Y. Huang, J. Kim, Y. Qiu, K. Nan, J. Kim, P. Gutruf, H. Luo, A. Zhao, K.-C. Hwang, Y. Huang, Y. Zhang, J. A. Rogers, *Sci. Adva.* **2016**, *2*, e1601014.
[22] H. D. McClintock, N. Doshi, A. Iniguez–Rabago, J. C. Weaver, N. T. Jafferis, K. Jayaram, R. J. Wood, J. T. B. Overvelde, *Adv. Funct. Mater.* **2021**, *31*, 2103428.

ADVANCED FUNCTIONAL MATERIALS

Supporting Information

for *Adv. Funct. Mater.,* DOI: 10.1002/adfm.202214897

Chiral Mechanical Metamaterials for Tunable Optical Transmittance

Antonio Elia Forte, David Melancon, Mohamed Zanati, Marta De Giorgi, and Katia Bertoldi**

Supporting Information

Chiral mechanical metamaterials for tunable optical transmittance

Antonio Elia Forte*†, David Melancon*, Mohamed Zanati, Marta De Giorgi, and Katia Bertoldi†

†Corresponding Authors' E-mails: bertoldi@seas.harvard.edu; antonio.forte@kcl.ac.uk

This PDF file includes:

Figs. S1 to S8
Table S1
Captions for Movies S1 to S2
References of the Supporting Information

Other supporting information for this manuscript include the following:

Movies S1 to S2

S1. Fabrication

The mechanical pixels considered in this study are constructed by assembling the five layers shown in Fig. S1a:

- (1): a 1/4 in. thick clear acrylic plate;
- (2): a 0.0015 in. thick mylar sheet with the spirals design laser cut out;
- (3): a 0.001 in. thick circular polarizing sheet;
- (4): a 1/4 in. thick clear acrylic plate;
- (5): a 0.001 in. thick polarizing sheet.

Layers (1)-(3) and (4)-(5) are first assembled together via bolts and glue and then the two parts are joined together by placing a thread through the bottom acrylic plate and the center of the spirals (see component (6) in Fig. S1b). More specifically, these eight steps are followed to fabricate our mechanical pixels (see Fig. S2 and Movie S1):

- **Step 1:** we cut layers (1) and (4) out of a 1/4 in. thick acrylic plate with a 150 W laser-cutter (PLS6.150D from Universal Laser Systems), using both lasers at 100% power, 3% speed, and 1000 pulses per inch.
- **Step 2:** we cut layers (3) and (5) out of a 0.001 in. thick polarizing sheet (Izgut High Contrast Linear Polarizing Film) using both lasers at 1% power, 5% speed, and 500 pulses per inch.
- **Step 3:** we cut the spirals (layer (2)) design out of a 0.0015 in. thick mylar sheet, using both lasers at 1.5% power, 5% speed, and 500 pulses per inch.
- **Step 4:** we clamp the layer (5) to layer (4) via bolts.
- **Step 5:** we clamp the mylar sheet with the spirals cut out (layer (2)) to the top fixture (layer (1)) via bolts.
- **Step 6:** we couple the circular polarizer (layer (3)) to the spirals (layer (2)) by applying a drop of cyanoacrylate glue (Krazy glue) in the center of the spirals (**Step 6a**) and firmly pressing down with the circular polarizer for 15 seconds to ensure bonding (**Step 6b**).
- **Step 7:** we position the bottom and top parts on top of each other such that the square and circular polarizers are initially aligned (**Step 7a**) and connect them via a friction-less thread (component (6)) (**Step 7b**). We fit plastic beads at the end of the thread to keep it in position and trim the excess length (**Step 7c**).
- **Step 8:** we place the optical metamaterial on a lighted surface (**Step 8a**) and apply a relative displacement between the top and bottom parts such that the thread pulls on the center of the spirals, engaging the rotation of the top, circular polarizer and changing the angle between the two polarizers.

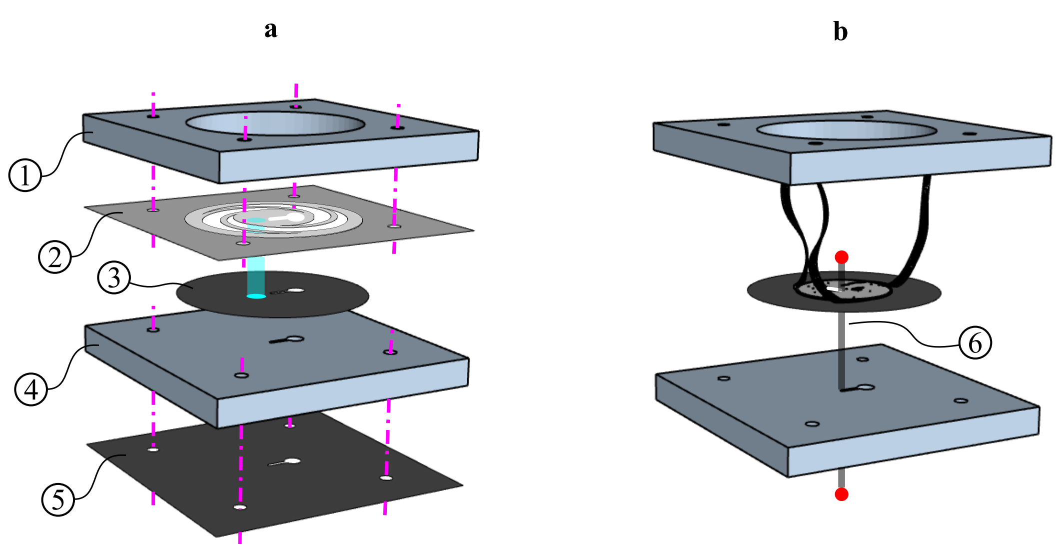

Fig. S1. Mechanical pixel. (a) Exploded view of our mechanical pixel. The dashed pink lines represent bolted connections and the shaded cyan area represents a glued connection. **(b)** Layers (1)-(3) and (4)-(5) are first assembled together via bolts and glue and then the two parts are joined together by placing a thread through the bottom acrylic plate and the center of the spirals (component (6)

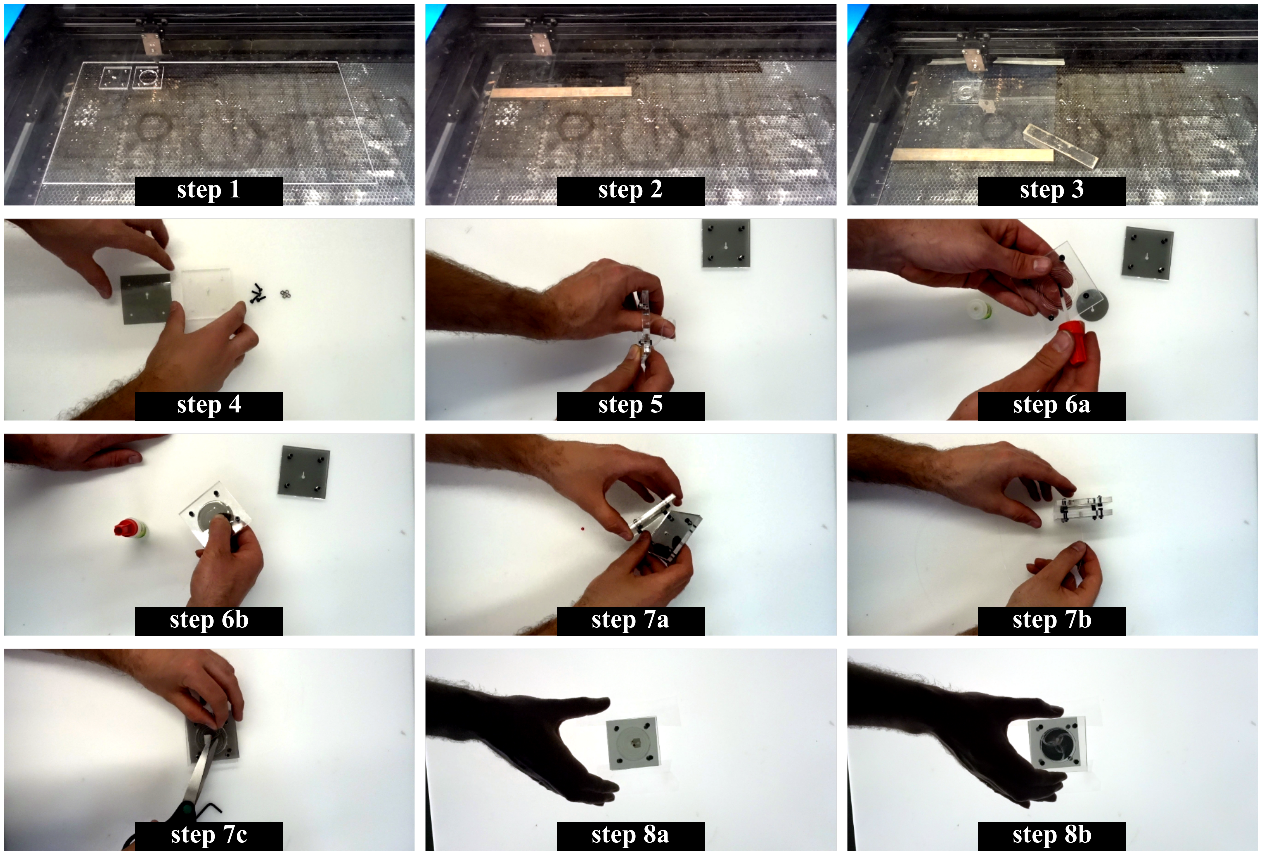

Fig. S2. Fabrication Snapshots of the eight steps required to fabricate and assemble a mechanical pixel.

S2. Testing

To measure the mechanical response of the spirals, (i.e., their ϕ-u_z relation) we fix the acrylic top plate (layer (1) in Fig. S1a) in space and pull on the thread (component (6) in Fig. S1b) with a digitally controlled linear stage (Thorlabs LTS150). In this way we apply a displacement $u_z \in [0, 30]$ mm to the spirals while leaving them free to rotate. To track the rotation (i.e., the angle ϕ), we monitor a reference line on the inner circle of the mylar sheet (visible in Fig. S1-a) and its position during the tests using a digital camera (SONY RX100 V) placed above the sample. We then use a Matlab script to control the linear stage in time as well as to extract the angle of rotation from the recorded videos.

S3. Color displays

A. Birefringent tape. Building on our platform, color displays can be realized by inserting a retarder (e.g., birefringent tape) between the polarizing films to induce a *double* refraction from the incident light passing through the system (1). To characterize the effect of the birefringent tape on the transmitted color, we start by superposing two polarizing films: an analyser that is free to rotate by ϕ_p and a polarizer that is fixed. As expected and shown in Fig. S3, at $\phi_p = 0$, the light is fully transmitted. However, as we increase ϕ_p, the polarizing films filter the intensity of the light according to Malus's law (2):

$$I_t = I_0 \cos^2(\phi_p), \quad [1]$$

where I_0 is the intensity of the light emitted from the source. Importantly, by introducing a birefringent tape, we exploit rotation to transition between different colors. As an example, we glue 12 pieces of birefringent tape (Izgut birefringent tape) on top of the fixed polarizer and below the rotating analyser and align their optical axis such that they are oriented at $\gamma_1 = k\pi/6$ (with $k \in [0, 11]$) with respect of the global x-axis of the system, where γ_1 is the angle between the tapes' optical axis and the global x-axis of the system (see Fig. S3a and Table S1 for details). As shown in Fig. S3a, we find that for the tapes with $\gamma_1 = \pi/6 + n\pi/2$ and $\pi/3 + n\pi/2$ (n being an integer) an increase in ϕ_p from 0° to 90° leads to a transition between the color blue and yellow, with colors that are brighter for $\gamma_1 = \pi/3 + n\pi/2$. Differently, for the transmitted color for tapes with $\gamma_1 = n\pi/2$ is white at $\phi_p = 0°$, light blue at $\phi_p = 45°$, black at $\phi_p = 90°$ and light yellow at $\phi_p = 135°$. To quantify these transitions in colors, we track the position of the central and the outer black dots in the recorded videos (using the function `imfindcircles` in Matlab), from which we can infer the angle ϕ_p. We then create sampling windows of 30x30 pixels positioned on each tape. We average the RGB values of the 900 pixels in each window and store it as a three element vector containing the values normalized between 0 and 1 for the red, green and blue channels. We then store these RGB vectors for each of the 12 layouts as a function of ϕ_p.

To increase the spectrum of colors that can be displayed, we consider layouts made of two (Fig. S3b) and three (Fig. S3c) layers of birefringent tape arranged on top of each other. These arrangements of tape are fully defined by γ_1 and the two additional angles γ_2 and γ_3, which denote the angle between the optical axis of the second and third layer of birefringent tape and the one underneath (see details in Figs. S3b-c and Table S1). More specifically, we consider 24 different tape layouts for two and three layers (Table S1). As shown in Figs. S3b-c, we find that both the number of layers and orientation of the birefringent tape affect the colors that are displayed. As such, these experiments provide a large database of 60 birefringent tape layouts that we then harness to design a mechanical color display.

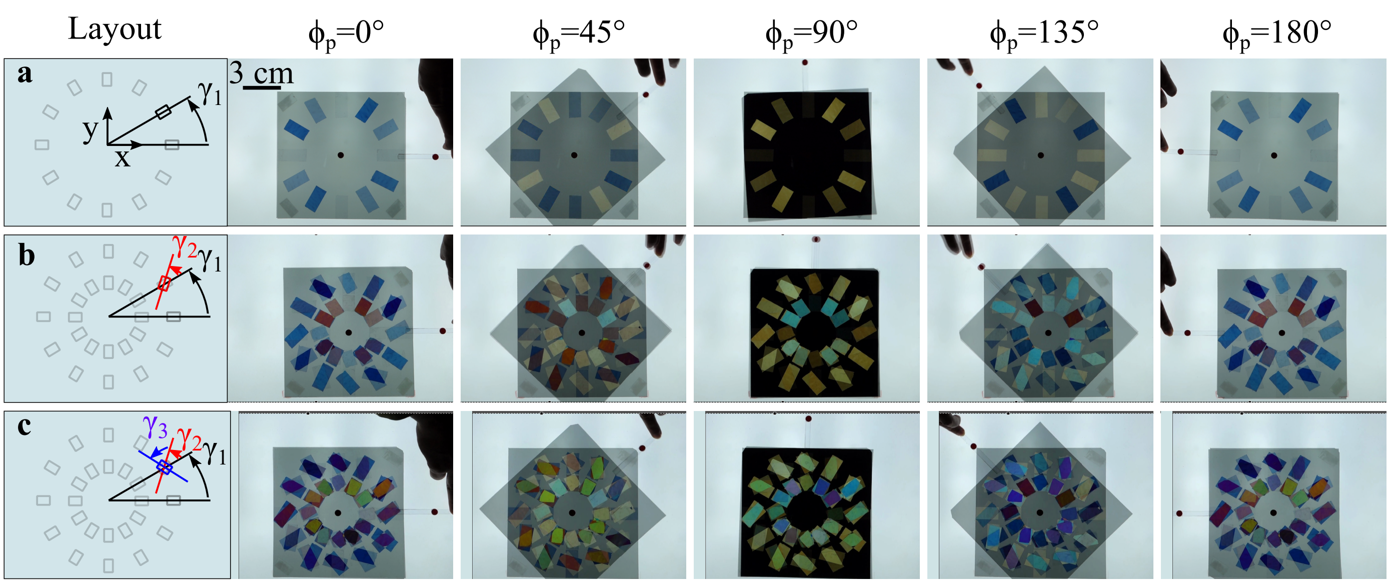

Fig. S3. Birefringent tape for color modulation. By changing the number of layers and the orientation of birefringent tape glued on top of the fixed polarized film, we obtain complex color moduluation. Here, we show top-view experimental pictures for $\phi_p = 0, 45, 90, 135$, and $180°$ for layouts with one **(a)**, two **(b)**, and three **(c)** layers of tape. See details of the tape layouts in Table S1

Table S1. Details of the birefringent tape layouts shown in Fig. S3.

1 layer $\gamma_1[°]$	2 layers $\gamma_1;\gamma_2[°]$	3 layers $\gamma_1;\gamma_2;\gamma_3[°]$
0	0; 0	0; 0; 15
30	30; 0	30; 0; 15
60	60; 0	60; 0; 15
90	90; 0	90; 0; 30
120	120; 0	150; 0; 30
150	150; 0	150; 0; 30
180	180; 15	180; 15; 15
210	210; 15	210; 15; 15
240	240; 15	240; 15; 15
270	270; 15	270; 15; 30
300	300; 15	300; 15; 30
330	330; 15	330; 15; 30
-	0; 30	0; 30; 15
-	30; 30	30; 30; 15
-	60; 30	60; 30; 15
-	90; 30	90; 30; 30
-	120; 30	120; 30; 30
-	150; 30	150; 30; 30
-	180; 45	180; 45; 15
-	210; 45	210; 45; 15
-	240; 45	240; 45; 15
-	270; 45	270; 45; 30
-	300; 45	300; 45; 30
-	330; 45	330; 45; 30

B. Fabrication of a color mechanical pixel. To fabricate a mechanical pixel able to manipulate colors, we follow the eight steps described in Section S1 (see Movie S1), but after **step 1** we apply n layers of birefringent tape (Izgut birefringent tape) on layer (4) (**step 1a**, Fig. S4), i.e., bottom fixture in Fig. S1a, and trim the excess (**step 1b**, Fig. S4). We place the optical metamaterial on a lighted surface (**step 2a**, Fig. S4) and apply a relative displacement between the top and bottom parts such that the thread pulls on the center of the spirals, engaging the rotation of the top, circular polarizer and changing the angle between the two polarizers (**step 2b**, Fig. S4).

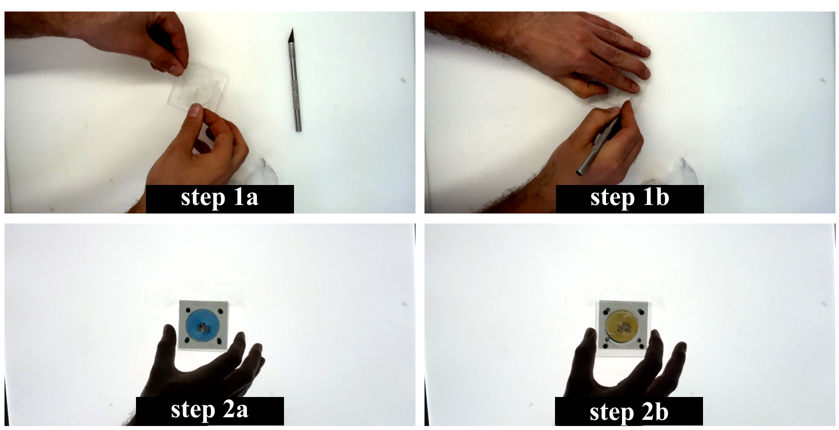

Fig. S4. Color display fabrication. Snapshots of the two additional steps required to modulate colors with our optical metamaterials.

S4. Additional results

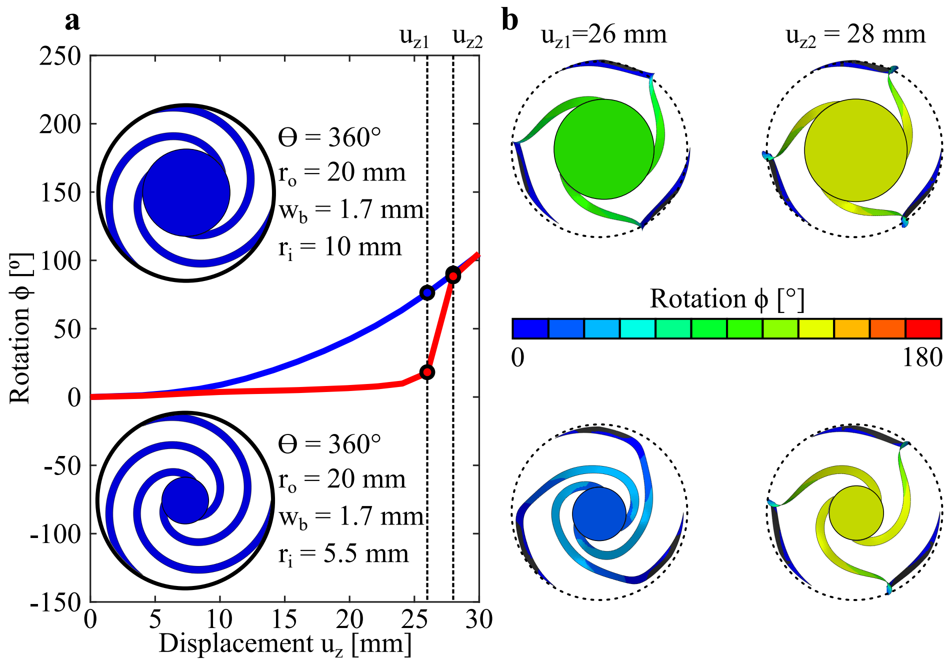

Fig. S5. Extension-twisting coupling. The extension-twisting coupling is mostly governed by the inner radius, r_i, and the angle spanned by the spirals, Θ (see Fig. 2 of the main manuscript). The inner radius, r_i, effectively dictates the length of the curved beams forming our unit cells. To give more insights into the effect of r_i on the behavior of the beams, here we focus on two unit cells with $(\Theta, r_o, w_b, r_i) = (360°, 20\text{ mm}, 1.7\text{ mm}, 10\text{ mm})$ and $(\Theta, r_o, w_b, r_i) = (360°, 20\text{ mm}, 1.7\text{ mm}, 5.5\text{ mm})$. **(a)** Rotation, ϕ, as a function of displacement, u_z, for the two unit cells. **(b)** FEM-predicted contour plots of the rotation, ϕ at $u_{z1} = 26$ mm and $u_{z2} = 28$ mm. This results indicate that for shorter beams (i.e., r_i=10 mm), the unit cell's twist increases smoothly with the out-of-plane displacement (see blue curves in (a)), a relation that was previously described in the literature for chiral metamaterials (3). Instead, longer curved beams (i.e., r_i=5.5 mm) are prone to buckling under twist, resulting in a sudden increase of ϕ upon loading (see red curve in (a)). In particular, for r_i=5.5 mm we see that the slender beams buckle around $u_{z1} = 26$ mm and suddenly increase the value of ϕ at around $u_{z2} = 28$ mm. Increasing Θ from $360°$ to $720°$ also increases the length of the beams. For unit cells with $\Theta = 720°$, we also have regions of the design space where twist increases smoothly with displacement (for shorter beams with $13 \leq r_i < 13.5$ mm—see yellow curves in Fig. 2b of the main manuscript) and sharply at a certain displacement because of buckling (for slender beams with $11 \leq r_i < 13$—see orange curves in Fig. 2b of the main manuscript). However, for extremely slender beams (i.e., $\Theta = 720°$ and $5.5 \leq r_i < 11$ mm—see purple curves in Fig. 2b of the main manuscript), a soft mode of deformation emerges where the system rotates only a small amount in the negative/clockwise direction (instead of the positive/counter-clockwise direction). The same mechanical behavior is displayed when we reduce the outer radius, r_o, which effectively changes the length scale of our system (see Fig. 2c of the main manuscript). Indeed, from $u_z = 0$ to $u_z = 15$ mm the curves of Fig. 2c are initially identical to the ones of Fig. 2b and then from $u_z = 15$ to $u_z = 30$ mm unlock larger attainable values of ϕ.

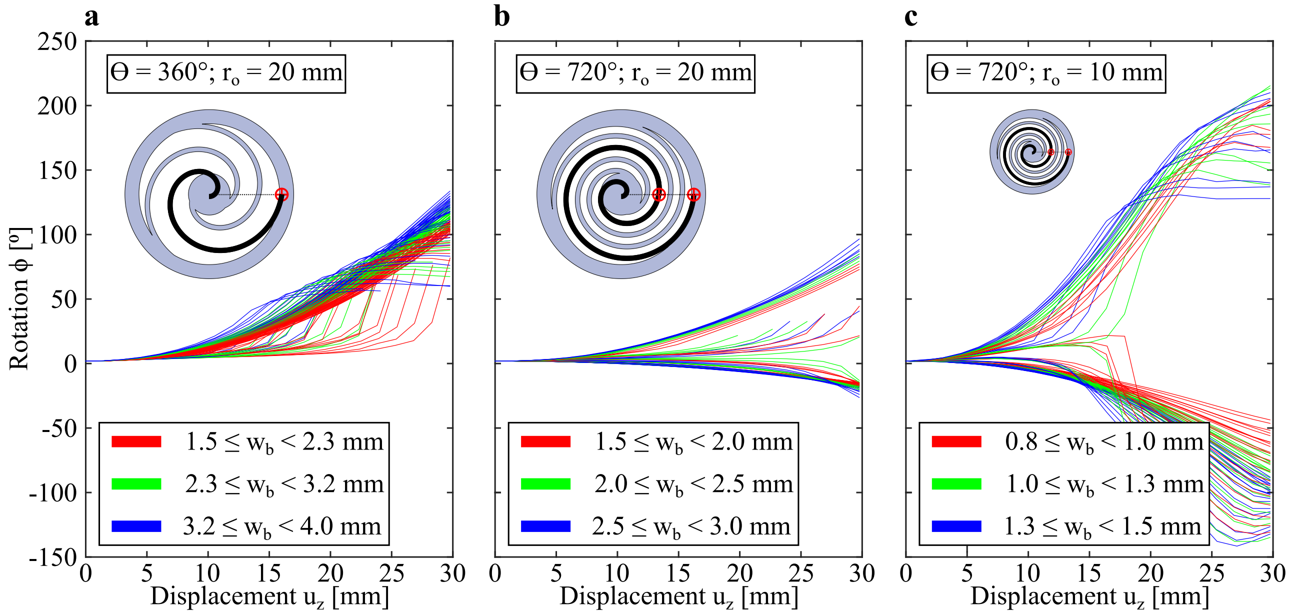

Fig. S6. FEM-predicted deformation of the spirals upon loading. Evolution of the twisting angle ϕ as a function of the applied displacement u_z for spirals with $t = 0.3$ mm, $r_i \in [2.8, 13.5]$ mm, $w_b \in [0.8, 4]$ mm and $(\Theta, r_o) = (360^\circ, 20\ \mathrm{mm})$ (a), $(720^\circ, 20\ \mathrm{mm})$ (b) , and $(720^\circ, 10\ \mathrm{mm})$ (c).

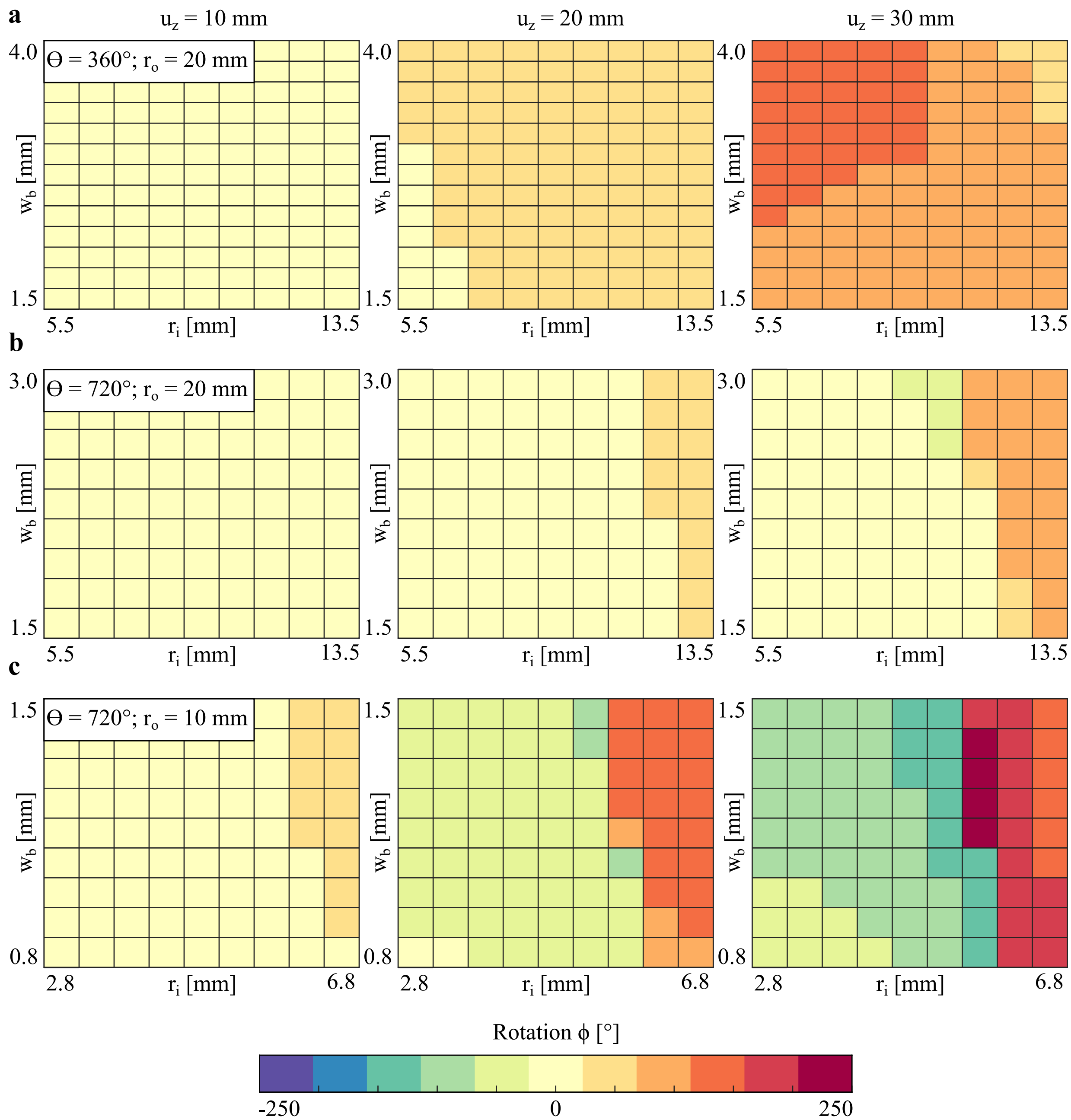

Fig. S7. Effect of geometric parameters on the twisting angle ϕ. Contour plots of the twisting angle ϕ as a function of the beam's width, w_b, and the spiral's inner radius, r_i at $u_z = 10$ (left), 20 (center), and 30 (right) mm for spirals with $(\Theta, r_o) = (360^\circ, 20\ \mathrm{mm})$ **(a)**, $(\Theta, r_o) = (720^\circ, 20\ \mathrm{mm})$ **(b)**, and $(\Theta, r_o) = (720^\circ, 10\ \mathrm{mm})$ **(c)**.

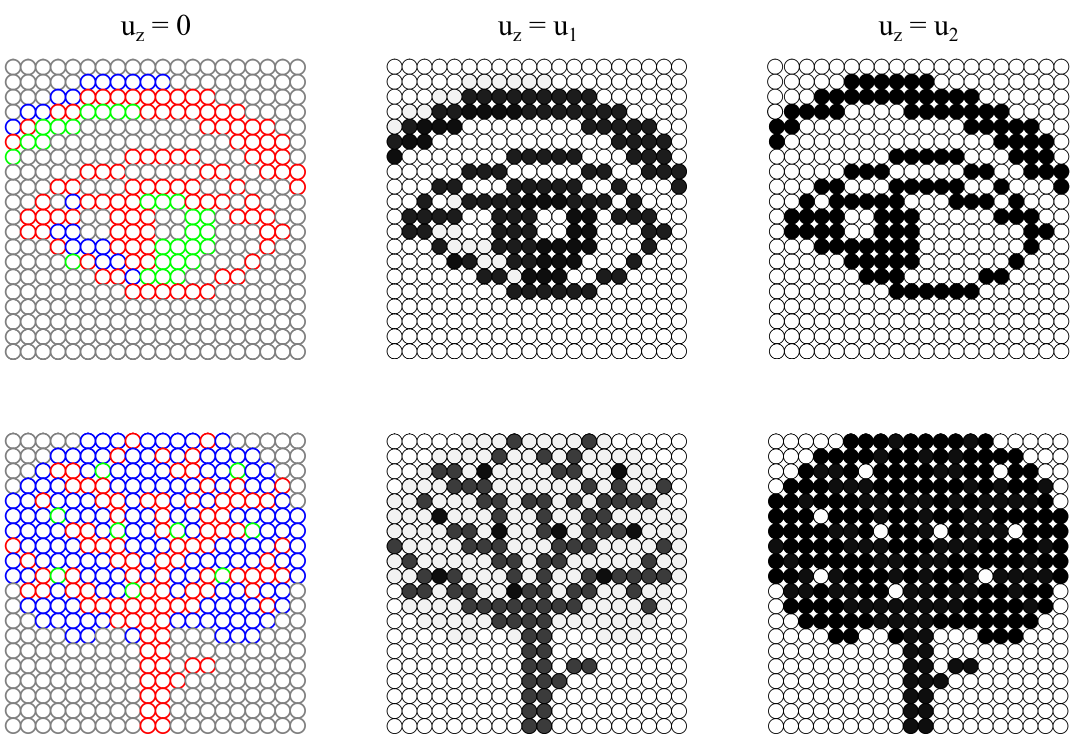

Fig. S8. High-resolution mechanical displays. Schematics of two 20×20 mechanical displays showing complex images at different state of deformation: **(a)** a white square transforming into an eye looking straight then sideways for $u_z = 0, u_1, u_2$, respectively and **(b)** a white square transforming into a naked tree then to a blossoming tree for $u_z = 0, u_1, u_2$, respectively.

Movie S1. Fabrication. In order to fabricate chiral mechanical metamaterials for tunable optical transmittance, we assemble polarizing films with mylar sheet with the spirals design laser cut out.

Movie S2. Mechanical displays. We perform FE analyses to predict the twist-extension relation of the spirals. We then search this database to design a mechanical display that shows a white square in the undeformed configuration and, upon out-of-plane loading, morphs from a black letter “L” on a white background to a black letter “S” on a white background.

References

1. A Beléndez, E Fernández, J Francés, C Neipp, Birefringence of cellotape: Jones representation and experimental analysis. *Eur. J. Phys.* **31**, 551–561 (2010).
2. E Collett, *Field guide to polarization*, SPIE field guides. (SPIE Press, Bellingham, Wash) No. v. FG05, (2005) OCLC: ocm58456547.
3. T Frenzel, M Kadic, M Wegener, Three-dimensional mechanical metamaterials with a twist. *Science* **358**, 1072–1074 (2017) _eprint: https://www.science.org/doi/pdf/10.1126/science.aao4640.